# Quantum-enhanced screened dark energy detection

Daniel Hartley,[1,*] Christian Käding,[2,3] Richard Howl,[4] and Ivette Fuentes[4]

[1] *Faculty of Physics, University of Vienna, Boltzmanngasse 5, 1090 Wien, Austria*

[2] *National Research University Higher School of Economics, 101000, Moscow, Russia*

[3] *School of Physics & Astronomy, University of Nottingham, University Park, Nottingham NG7 2RD, United Kingdom*

[4] *School of Mathematical Sciences, University of Nottingham, University Park, Nottingham NG7 2RD, United Kingdom*

(Dated: September 6, 2019)

arXiv:1909.02272v1 [gr-qc] 5 Sep 2019

## Abstract

We propose an experiment based on a Bose-Einstein condensate interferometer for strongly constraining fifth-force models. Additional scalar fields from modified gravity or higher dimensional theories may account for dark energy and the accelerating expansion of the Universe. These theories have led to proposed screening mechanisms to fit within the tight experimental bounds on fifth-force searches. We show that our proposed experiment would greatly improve the existing constraints on these screening models by many orders of magnitude, entirely eliminating the remaining parameter space of the simplest of these models.

* Corresponding author: daniel.hartley@univie.ac.at

General relativity (GR) has remained a tremendously successful theory, producing accurate physical predictions consistent with the barrage of experiments and observations conducted over the last century. Despite this success, there are still many open problems within GR and apparent limitations of the theory itself. Amongst modified theories of gravity aiming to address these problems, scalar-tensor theories (e.g. Brans-Dicke theory [1], see also [2]) are some of the most widely studied. Modified theories of gravity like $f(R)$-gravity can additionally be shown to be equivalent to scalar-tensor theories, and higher dimensional theories (e.g. string theory) predict the existence of effective scalar field modes in 4-dimensional spacetime due to compactifications of the extra dimensions [3].

Modifications of gravity gained even greater attention after the accelerated expansion of the Universe was discovered [4, 5] and the puzzle of dark energy (DE) - the energy that supposedly drives this expansion - arose. Consequently, there have been several proposed explanations for the nature of DE based on scalar-tensor theories (see e.g. [6, 7] for an overview of models). Some of these models are predicted to cause a fifth force, which is in contradiction with observations and experiments [8–10]. Consequently, some of these models have already been ruled out by observations [11]. However, models with a so-called "screening mechanism" [12] have features that supress the effects of the additional scalar fields in regions of high matter density. A screening mechanism would allow additional scalar fields to contribute to dark energy while the coupling to matter as a fifth force still evades experimental constraints.

Cold atom systems have proven to be invaluable tools in precision metrology. From practical applications such as ultra-high precision clocks [13] to more fundamental experiments searching e.g. for deviation from the equivalence principle [14–16], the high degree of control and low internal noise afforded by cold atom systems makes them an ideal testing ground. Many scalar-tensor theories assume a conformal coupling between the metric tensor and the scalar field, and cold atom systems have been found to be well suited to studying these particular models in experiments (e.g. in atom interferometers [17, 18]) and analogue gravity simulations [19]. Atom interferometry experiments currently provide the tightest constraints on some of these models [12, 20].

In this Letter, we propose using a guided Bose-Einstein condensate (BEC) interferometer scheme to further constrain these conformally coupled screened scalar field models. Guided is used in this context to refer to atoms held in a trap for all or most of the interferometer

scheme, rather than being in free fall. For this scheme, we consider a guided BEC interferometer as currently demonstrated in experiments. The main advantage of this scheme is a longer integration time: a trapped BEC can be held near a source object for much longer than atoms in a ballistic trajectory. We show that the constraints on the above screened scalar field models could be improved by many orders of magnitude.

The models we consider here come from scalar-tensor theories of gravity [2]. As stated above, an additional scalar field $\Phi$ may be coupled to the metric tensor conformally in these theories, such that ordinary matter fields evolve according to the conformal metric

$$\tilde{g}_{\mu\nu} = A^2(\Phi)\, g_{\mu\nu} \tag{1}$$

for some conformal factor $A^2(\Phi)$, where $g_{\mu\nu}$ is the normal GR metric. The equilibrium state of the $\Phi$ field is determined by minimising an effective potential [7, 12, 21]

$$V_{\text{eff}}(\Phi) = V(\Phi) + A(\Phi)\,\rho, \tag{2}$$

where $V(\Phi)$ is the self-interaction potential of the model and $\rho$ is the ordinary matter density.

We specifically consider two prominent examples of fifth force models with screening mechanism, namely the chameleon field [21, 22] and the symmetron field (first described in [23–28] and introduced with its current name in [29, 30]). These models have been investigated in atom interferometry experiments as the thick wall of a vacuum chamber can shield its interior from outside effects [17, 31], allowing the ultra-high vacuum to simulate the low density conditions of empty space resulting in long range (and thus measurable) chameleon or symmetron forces.

The chameleon field model is described by the conformal coupling [21]

$$A^2(\Phi) = \exp\left[\Phi/M_c\right] \tag{3}$$

and the potential

$$V(\Phi) = \Lambda^4 \exp\left[\Lambda^n/\Phi^n\right]. \tag{4}$$

The parameter $M_c$ determines the strength of the chameleon-matter coupling. This parameter is essentially unconstrained but is plausibly below the reduced Planck mass $M_{Pl} \approx 2.4 \times 10^{18}$ GeV/$c^2$. The self-interaction strength $\Lambda$ determines the contribution of the chameleon field to the energy density of the Universe, as the potential can be expanded

as $V \approx \Lambda^4 + \Lambda^{4+n}/\Phi^n$. This energy density can drive the accelerated expansion of the Universe observed today if $\Lambda = \Lambda_{DE} \approx 2.4$ meV. Finally, different choices of the parameter $n$ define different models, where $n \in \mathbb{Z}^+ \cup \{x : -1 < x < 0\} \cup 2\mathbb{Z}^- \setminus \{-2\}$ produces valid models with screening mechanisms. The two most commonly studied chameleon models are those where $n = 1$ or $-4$ [12].

The effective mass of the chameleon field in equilibrium is determined by the minimum of its effective potential, i.e. $m_c^2 = |\partial^2 V_{\text{eff}}/\partial\Phi^2|_{\Phi=\Phi_{\min}}$. The position of the effective potential minimum (and thus effective mass) depends on the ordinary matter density $\rho$ (see Appendix A for a detailed demonstration). In regions of low density, e.g. the intergalactic vacuum, the chameleon is light and mediates a long range force. In regions of high density, e.g. in a laboratory, the chameleon becomes massive and the force becomes short-ranged, making it challenging to detect with fifth force tests.

The symmetron model has a conformal coupling and a potential given by [29]

$$A^2(\Phi) = \exp\left[\Phi^2/2M_s^2\right] \tag{5}$$

and

$$V(\Phi) = -\frac{\mu^2}{2}\Phi^2 + \frac{\lambda_s}{4}\Phi^4 \tag{6}$$

respectively. As for the chameleon, $M_s$ gives the symmetron-matter coupling and $\lambda_s$ determines the self-interaction strength. Unlike the chameleon, the symmetron effective potential has a $\mathbb{Z}_2$ symmetry which can be spontaneously broken in environments of low matter density (see Appendix A). This allows the symmetron to obtain a non-vanishing effective mass in regions where the ambient matter density is below the critical density $\rho^* = \mu^2 M_s^2$. The symmetron field has a vanishing vacuum expectation value in high density regions ($\rho > \rho^*$) and thus a vanishing force. Consequently, the parameter $\mu$ determines the scale of the symmetron-matter decoupling.

We propose to use a BEC interferometer held near some source mass to constrain the chameleon and symmetron models (Fig. 1). The lowest order gravitational effect of the source mass is a gravitational redshift, which manifests as a position dependent global phase. The lowest order potential fifth force effect is a modification of this global phase by a position dependent value. This total global phase $\theta$ is given by (see Appendix B)

$$\theta(r) = \frac{mc^2T}{2\hbar}\left[\frac{r_s}{r} - 2\log A(\Phi(r))\right] \tag{7}$$

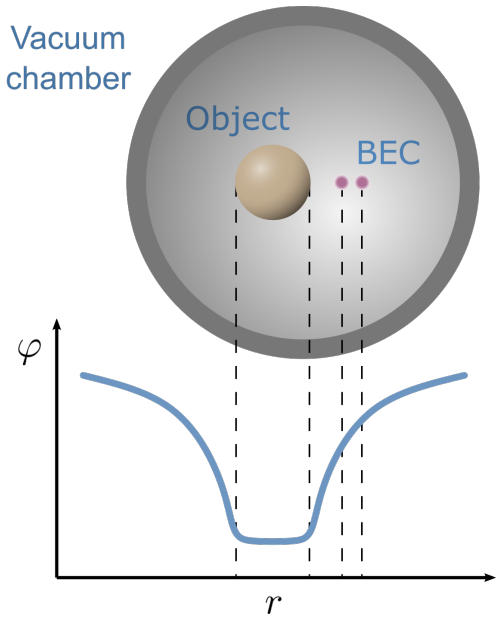


FIG. 1: A schematic diagram of the vacuum chamber overlaid on the field profile of a chameleon field around a spherical source object. The separation of the BEC components is greatly exaggerated.

where $r_s$ is the Schwarzschild radius of the source object, $m$ is the mass of each atom in the BEC, $T$ is the time and $A$ is the conformal factor defined as above. A BEC coherently split into parts would measure the phase gradient and thus field gradient in an interference measurement. The other contributions from the environment (e.g. the gravity of the Earth) could be subtracted with differential measurements or a dual interferometer scheme where measurements are performed near to and far from the source object.

BEC-based interferometers are not a new concept, and have already been proposed and demonstrated (e.g. [32–36], see also [37] and references therein). Coherent splitting of a BEC into spatially separated clouds has been implemented both with atom chips [32, 34, 38] (chips printed with an electrode structure allowing for the generation of magnetic and radio-frequency fields very close to an atom cloud) and in free space [39]. Recombination and interference of the separated clouds is typically achieved by turning the trapping potential off and letting the clouds expand into each other as they fall [37]. An alternative scheme has been recently realised, where the two condensate parts are brought into contact via Josephson tunnelling through a low potential barrier [40]. This acts as a beam splitting operation, and the interference contrast is projected onto a mean atom number difference

between the two wells.

The optimal sensitivity of a measurement maximised over all possible measurement schemes is given by the quantum Fisher information (QFI) through the quantum Cramér-Rao bound (QCRB) [41–43]. Since the QFI gives the best possible sensitivity in estimating a parameter, optimised over all possible forms of measurement, the QCRB trivially follows as

$$(\Delta\kappa)^2 \geq \frac{1}{NH(\kappa)} \tag{8}$$

where $\Delta\kappa$ is the absolute error in estimating the parameter $\kappa$ due to some measurement, $H(\kappa)$ is the QFI for estimating the parameter $\kappa$ and $N$ is the number of measurements performed.

Gaussian states cover the majority of easily experimentally accessible states such as coherent states, thermal states and squeezed states. Calculating the QFI for Gaussian states is simple as Gaussian states have a straightforward description in terms of their first and second moments [44–46].

Let $\theta_-$ be the accumulated phase difference between two arms of a BEC interferometer. The QFI for estimating $\theta_-$ with a fully condensed $\mathcal{N}_0$-atom BEC is given by

$$H(\theta_-) = \mathcal{N}_0 \tag{9}$$

which scales with the standard quantum limit (SQL) [47].

We now consider some experimental limitations to the schemes proposed in this Letter and use these to calculate the expected sensitivity of our schemes to constraining the chameleon and symmetron models. Typical BEC experiments condense clouds consisting of $10^4 - 10^6$ atoms, although condensates of up to $10^8$ atoms have been demonstrated with sodium [48], and up to $10^9$ atoms has been demonstrated with hydrogen [49, 50]. For estimating the sensitivity of this detector, we assume an initial BEC with $10^6$ atoms.

The maximum integration time of our proposed detector is set by the mutual coherence time of the components of the split BEC. Mutual coherence times up to 500 ms have been demonstrated with atom chips [51, 52], so we will estimate the integration time of our detector to be 500 ms.

We do not consider the effects of technical noise in the trapping potential or other sources of experimental noise. While we expect that these sources of noise will contribute substantially to the achievable sensitivity of any detector, any substantive analysis will strongly

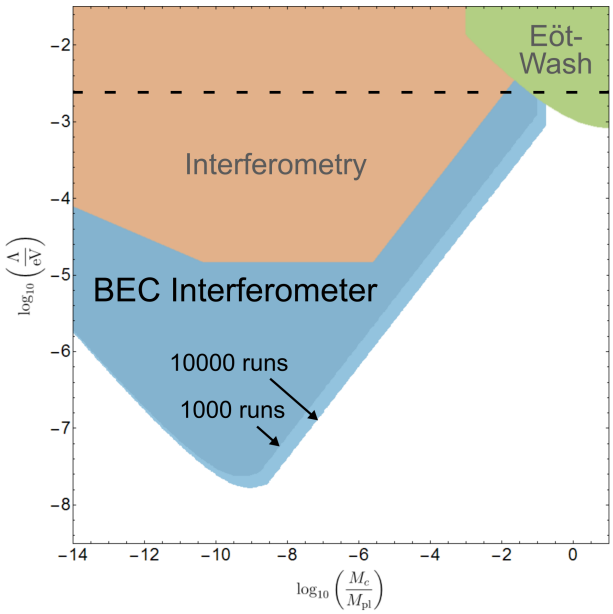


FIG. 2: Constraints for the parameter space of the chameleon model $n = 1$. The brown area corresponds to constraints from atom interferometry and the green area to those from Eöt-Wash experiments [12, 20]. The dotted line indicates the DE scale $\Lambda = 2.4$ meV. New constraints predicted in this work are coloured in blue, where dark blue corresponds to 1000 runs and light blue corresponds to 10000 runs.

depend on the details of the experimental implementation which we also leave to future work.

The expected new bounds on the chameleon and symmetron models from an implementation of our proposed schemes are presented in Figs. 2 - 4. Together with the numbers given above, we use the same experimental dimensions as in [53] for ease of comparison. Specifically, we consider a spherical vacuum chamber of radius $L = 5$ cm and vacuum pressure $6 \times 10^{-10}$ Torr. The source object is an aluminium sphere with a radius of $R = 9.5$ mm. The effective distance between the object and the BEC is 8.8 mm, and we assume that the two parts of the BEC are split by 100 $\mu$m. With clever trap positioning, the distance between the object and the BEC may eventually be limited by the strength of the van der Waals or Casimir-Polder forces, but these are not relevant at the 10 mm scale.

Fig. 2 shows the predicted new constraints for one of the most popular screening models - the chameleon with $n = 1$. There it can be seen that the BEC interferometry scheme would be able to improve existing constraints for this model by up to 3 orders of magnitude

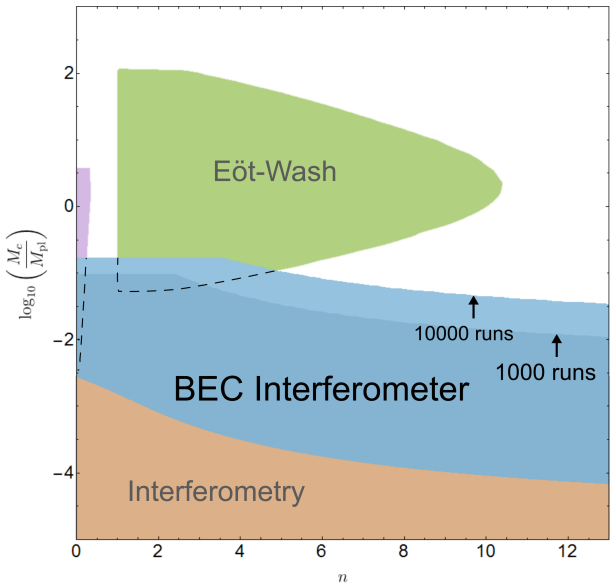


FIG. 3: Constraints for the value of $M_c$ for positive $n$ chameleon models at $\Lambda = 2.4$ meV. The brown area corresponds to constraints from atom interferometry, the green area to those from Eöt-Wash experiments, and the violet area represents constraints from astrophysics [12, 20]. New constraints predicted in this work are coloured in blue, where dark blue corresponds to 1000 runs and light blue corresponds to 10000 runs.

and close the gap between former interferometry and Eöt-Wash experiment constraints on the DE scale $\Lambda = 2.4$ meV. This amounts to ruling out the simplest chameleon model as a model of dark energy.

Figure 3 shows constraints for the value of $M_c$ over different values of positive $n$ chameleon models and for $\Lambda = \Lambda_{\rm DE} = 2.4$ meV. Our scheme would improve existing interferometry constraints by more than 2 orders of magnitude and close the gap to Eöt-Wash for $n \leq 5$.

The predicted constraints on the parameter space of the symmetron model are shown in Fig. 4. We expect that our proposed experiment would improve the existing constraints by between 16 and 26 orders of magnitude in $\lambda$ across the entire accessible range of $M_s$.

For a summary of the accessible areas of and detailed constraints on the parameter space for both the chameleon and symmetron models, see Appendix C.

While we have only considered chameleon and symmetron screening models, it should be stressed that constraints for any other type of conformally coupled scalar field could be obtained in a similar manner, e.g. for galileons [54] or dilatons [55, 56].

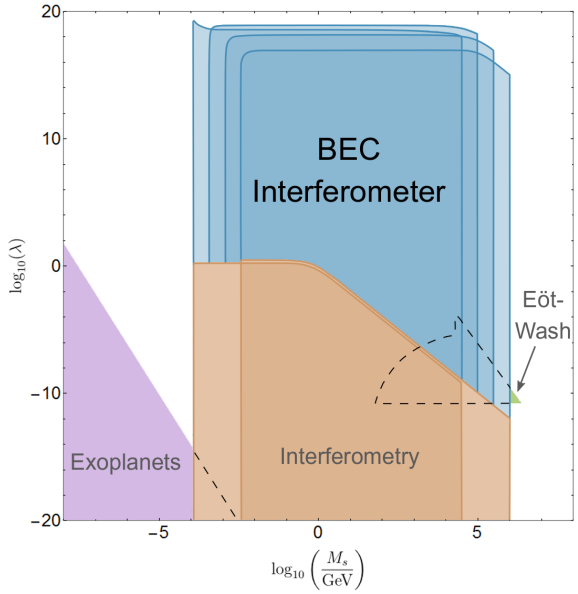


FIG. 4: Constraints for the parameter space of the symmetron model. The brown area corresponds to constraints from atom interferometry, the green area to those from Eöt-Wash experiments, and the violet area represents constraints from exoplanet astrophysics [12, 20]. New constraints predicted in this work for a BEC interferometer are coloured in blue. Different shades of blue correspond to $\mu = 10^{-4}$, $10^{-4.5}$, $10^{-5}$ and $10^{-5.5}$ eV in natural units respectively.

To bring this proposal into reality, future work will focus on optimising the experimental implementation. Any subsequent implementation of our proposal will either discover $n = 1$ chameleon fields at the cosmological energy density or completely rule them out, along with greatly improving the bounds on other screened scalar models.

## ACKNOWLEDGMENTS

The authors thank C. Burrage, B. Elder and A. L. Báez-Camargo for helpful comments, and C. Burrage and J. Sakstein for providing their constraint plot files. The authors acknowledge financial support from the Austrian Science Fund (FWF) through project code W 1210-N25, the University of Nottingham, and the John Templeton Foundation through Grant No. 58745. The opinions expressed in this publication are those of the authors and do not necessarily reflect the views of the John Templeton Foundation.

## Appendix A: Effective potentials for the chameleon and symmetron models

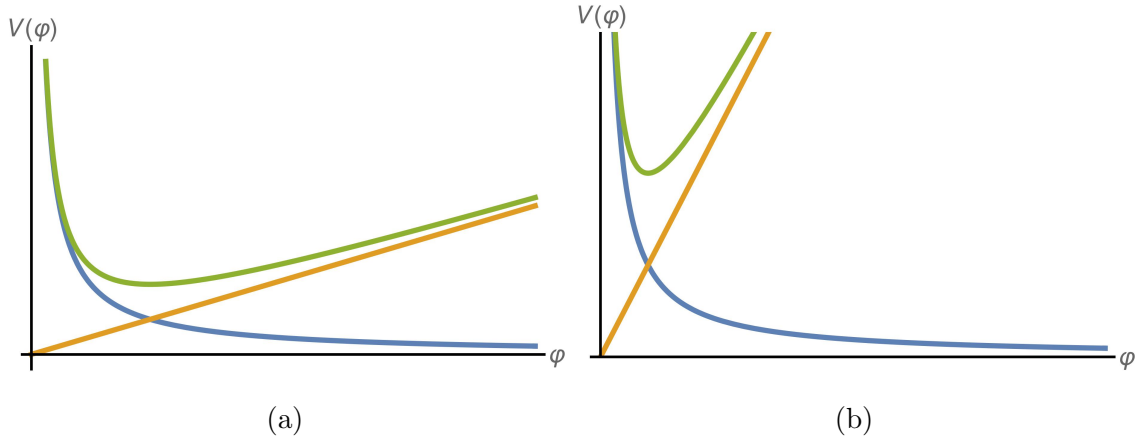


FIG. 5: $n = 1$ chameleon effective potential for high (left) and low (right) ordinary matter densities plotted in green, with its components plotted in blue and orange.

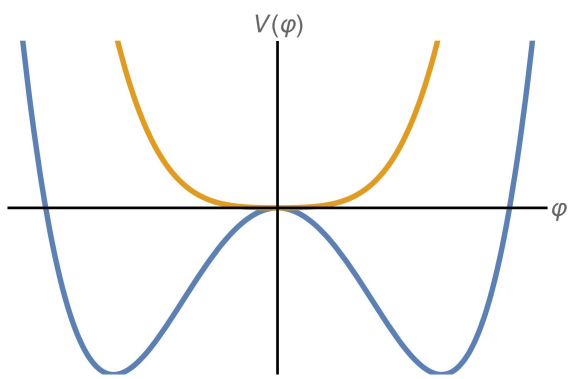


FIG. 6: Symmetron effective potential for high (blue) and low (orange) ordinary matter densities.

Fig. 5 compares the chameleon effective potential $V_{\text{eff}}$ (in green) in high and low density environments for the $n = 1$ chameleon. The effective potential is given to lowest order by

$$V_{\text{eff}}(\Phi) = \frac{\Lambda^{4+n}}{\Phi^n} + \frac{\rho}{2M_c}\Phi + \mathcal{O}\left(\frac{\Phi^2}{M_c^2}\right). \tag{A1}$$

These first two components are plotted in blue and orange respectively for low (Fig. 5a) and high (Fig. 5b) values of $\rho$. It is reasonable to ignore higher order terms in $\Phi/M_c$ as any fifth force effect measured on or near the Earth must be perturbative to be consistent with

experimental observations. The effective mass of excitations of the chameleon field is given by

$$m_c^2 = \left| \frac{\partial^2 V_{\text{eff}}}{\partial \Phi^2} \right|_{\Phi=\Phi_{\min}} = 2\Lambda^5 \left( \frac{\rho}{2M_c\Lambda^5} \right)^{3/2} \tag{A2}$$

for $n = 1$, which clearly scales with $\rho$. Therefore, any chameleon force will be screened in high density environments.

Fig. 6 compares the symmetron effective potential for high (orange) and low (blue) density environments. The effective potential is given by

$$V_{\text{eff}}(\Phi) = \frac{1}{2}\left( \frac{\rho}{M_s^2} - \mu_s^2 \right)\Phi^2 + \frac{\lambda_s}{4}\Phi^4 \tag{A3}$$

from which it is obvious that the $\mathbb{Z}_2$ symmetry ($\Phi \to -\Phi$) is broken when the coefficient of the quadratic term in $\Phi$ is negative. This occurs at the critical density $\rho^* = \mu_s^2 M_s^2$. Above this density (Fig. 6, orange curve), the minima of $V_{\text{eff}}$ are degenerate at $\Phi = 0$ so there is no fifth force. Below this density (Fig. 6, blue curve), the minima become non-degenerate and non-zero at an effective mass of

$$m_s^2 = 2\left( \mu_s^2 - \frac{\rho}{M_s^2} \right). \tag{A4}$$

**Appendix B: Derivation of the lowest order effect of a conformally coupled screened scalar effect on a bosonic field**

We begin by modelling our BEC as an interacting massive scalar Bose field $\hat{\Phi}(\boldsymbol{x}, t)$ in a covariant formalism to introduce the background metric in a natural way, following the approach of [19, 57, 58]. Note that we do not assume that the BEC has "relativistic" properties such as large excitation energies (i.e. mass energy), high flow velocities (i.e. speed of light) or a strong interaction strength etc., and will later explicitly make "non-relativistic" restrictions.

Following the above references, we describe the evolution of the field operator $\hat{\Phi}$ with the Lagrangian density

$$\mathcal{L} = -\sqrt{-g}\left\{ \partial^\mu \hat{\Psi}^\dagger \partial_\mu \hat{\Psi} + \left( \frac{m^2c^2}{\hbar^2} + V \right)\hat{\Psi}^\dagger\hat{\Psi} + U \right\}, \tag{B1}$$

where $V$ is the external potential, $U$ is the interaction potential and $g_{\mu\nu}$ is the metric of the background (in general curved) spacetime with determinant $g$. As is standard in BEC

literature [59, 60], we consider only the leading order 2-particle contact interactions and approximate the interaction strength as

$$U = \frac{\lambda}{2}\hat{\Psi}^\dagger\hat{\Psi}^\dagger\hat{\Psi}\hat{\Psi}. \tag{B2}$$

The interaction strength $\lambda$ can be related to the s-wave scattering length $a_s$ by

$$\lambda = 8\pi a_s. \tag{B3}$$

We can rewrite the field operator $\hat{\Psi}$ as

$$\hat{\Psi} = \hat{\phi}e^{imc^2t/\hbar}. \tag{B4}$$

We will later make the assumption that time derivatives of $\hat{\phi}$ are small, i.e. the excitations described by $\hat{\phi}$ have non-relativistic energies.

The appropriate background metric near a sphere of radius $R$ and mass $M$ sourcing screening for the assumed screened scalar field has the line element

$$ds^2 = e^{\zeta^2(r)}\left[-f\left(r\right)dt^2 + f^{-1}\left(r\right)dr^2 + r^2 d\Omega^2\right] \tag{B5}$$

where $f\left(r\right) = 1 - r_s/r$, $r_s = 2GM/c^2$ is the Schwarzschild radius of the object and the conformal factor $A$ has been rewritten as $A^2\left(\Phi\right) = \exp\left[\zeta^2\left(\Phi\right)\right]$ for notational convenience. Eq. (B5) reduces to the Schwarzschild metric when $\zeta^2 \to 0$. The gravitational effect of the Earth is ignored; it is assumed that this can be accounted for either with differential measurements with and without the mass or through a dual interferometer scheme or simply by splitting the interferometer horizontally.

We now convert this Lagrangian to a Hamiltonian density (for readability and ease of interpretation) and make the following assumptions:

1. $|\zeta^2| \ll 1$,

2. $r_s \ll r$,

3. $\left|\partial_t\hat{\phi}\right|/c \ll \left|\partial_i\hat{\phi}\right|$ and

4. $\hbar^2\left|\partial_i\hat{\phi}^\dagger\partial_i\hat{\phi}\right| \ll m^2c^2\hat{\phi}^\dagger\hat{\phi}$,

where $i$ runs over spatial indices. To lowest order in $\zeta^2$ and $r_s/r$, the resulting Hamiltonian density is

$$\mathcal{H} = \frac{\hbar^2}{2m}\sum_i \partial_i\phi^\dagger\partial_i\phi + V_{eff}\hat{\phi}^\dagger\hat{\phi} + \frac{1}{2}\lambda_{NR}\hat{\phi}^\dagger\hat{\phi}^\dagger\hat{\phi}\hat{\phi}, \tag{B6}$$

where

$$V_{eff} = V_{NR} + \frac{1}{2}mc^2\left[\zeta^2 - \frac{r_s}{r_{avg}}\right]. \tag{B7}$$

The potentials have been rescaled in the form

$$V_{NR} = \frac{V}{2m}\,,\ \lambda_{NR} = \frac{\lambda}{2m} \tag{B8}$$

as these are the form of the external potential and interaction strength that usually appear in the Gross-Pitaevskii equation (GPE) [59, 60]. The interaction strength $\lambda_{NR}$ is usually written as $g$ (e.g. in [59]), but we avoid this notation here to avoid confusion with the background spacetime metric.

We have defined $r_{avg}$ as the mean distance of the BEC from the center of the source mass, and expanded $r_s/r$ as

$$\frac{r_s}{r} = \frac{r_s}{r_{avg}+r'} = \frac{r_s}{r_{avg}}\left(1 - \frac{r'}{r_{avg}} + \cdots\right). \tag{B9}$$

We can neglect all terms except the first if the BEC trap geometry has a negligible extent in the direction perpendicular to the source mass field gradient. For example, the BEC could be trapped with a cigar-shaped trapping potential oriented perpendicularly to the source mass.

The total field $\hat{\phi}$ can be written in terms of momentum eigenmodes as [59]

$$\hat{\phi}\left(\boldsymbol{r},t\right) = \left[\Psi_0\left(\boldsymbol{r}\right) + \hat{\vartheta}\left(\boldsymbol{r},t\right)\right]e^{-i\mu t/\hbar}, \tag{B10}$$

where $\Psi_0$ corresponds to the momentum ground state, $\mu$ is the chemical potential and $\hat{\vartheta}$ contains all higher order modes. We make the Bogoliubov approximation and also assume that the excited modes of the field are negligibly occupied. If the potentials $V_{NR}$ and $\lambda_{NR}$ are stationary, then the equation of motion for $\Psi_0$ derived from the above Hamiltonian density is

$$\left[-\frac{\hbar^2}{2m}\nabla^2 + V_{eff} - \mu + \lambda_{NR}\left|\Psi_0\left(\boldsymbol{r}\right)\right|^2\right]\Psi_0\left(\boldsymbol{r}\right) = 0. \tag{B11}$$

This is the time-independent GPE with the potential replaced by the effective potential $V_{eff}$. Since the screened scalar field contribution to $V_{eff}$ is approximately constant across

the width of the BEC, this GPE can be solved by splitting the chemical potential into $\mu = \mu_0 + \mu_I$ where $\mu_0$ is the chemical potential when $V_{eff} \to V_{NR}$. The extra term is then given by

$$\mu_I = \frac{1}{2} mc^2 \left[ \zeta^2 - \frac{r_s}{r_{avg}} \right]. \tag{B12}$$

Thus, the lowest order effect on the BEC ground state is a shift in the chemical potential, i.e. a phase shift. Physically, this phase is the gravitational red-shift due to the source mass, and the lowest order contribution of the screened scalar field is a modification of this red-shift. It is also worth noting that this phase shift appears in both the ground state and all excited modes of the BEC in a basis independent way.

### Appendix C: Analysis of the constraint plots in the main text

The constraints plotted in Figures 2-4 in the main text are derived from the quantum Cramer-Rao bound for estimating the phase difference in an interferometer. This bound is given by

$$(\Delta\theta_-)^2 \geq \frac{1}{\sqrt{NH(\theta_-)}}. \tag{C1}$$

Assuming a null measurement, the bounds on the screening models are given by

$$\frac{1}{\sqrt{NH(\theta_-)}} \geq \frac{mc^2 T}{2\hbar} \left( \zeta^2(r_1) - \zeta^2(r_0) \right) \tag{C2}$$

for phases measured at $r_0$ and $r_1$.

#### 1. Chameleon constraints, Figures 2 and 3 in the main text

There are three major sections in the BEC interferometer constraints in Fig. 4; the negatively sloped section where $M_c/M_{\rm pl} < 10^{-10}$, the vertical lines bounding the region on the large $M_c$ side of the figure, and the positively sloped section between them.

In the limit of an infinitely wide vacuum chamber, the $n = 1$ chameleon field in the (non-perfect) vacuum has an effective mass

$$m_\infty^2 = 2\Lambda^5 \left( \frac{\rho_\infty}{2M_c\Lambda^5} \right)^{3/2} \tag{C3}$$

where $\rho_\infty$ is the matter density of the vacuum. When the chameleon field is screened within the source mass, the constraint resulting from a null measurement is given by

$$\frac{1}{\sqrt{NH\left(\theta_-\right)}} > \frac{mc^2T}{2\hbar}\sqrt{\frac{2\Lambda^5}{M_c}}\left(\frac{1}{\sqrt{\rho_\infty}}-\frac{1}{\sqrt{\rho_{obj}}}\right)Re^{m_\infty R/\hbar}\left|\frac{e^{-m_\infty r_1/\hbar}}{r_1}-\frac{e^{-m_\infty r_0/\hbar}}{r_0}\right| \tag{C4}$$

where $\rho_{\rm obj}$ is the density of the source object; this corresponds to the negatively sloped section of the Figure 2 constraints.

For larger values of $M_c$, the infinite vacuum chamber approximation does not hold as the Compton wavelength of the equilibrium chameleon becomes larger than the size of the vacuum chamber. In this case, the field equilibrium inside the vacuum chamber is instead described by [61]

$$\varphi_\infty \to \xi\left(n(n+1)\Lambda^{4+n}R^2\right)^{\frac{1}{n+2}}, \tag{C5}$$

where $\xi = 0.55$ is a fudge factor given by the chamber's spherical geometry and vacuum density. The effective mass is set to the radius of the vacuum chamber $m_\infty \to \hbar/R_{\rm vac}$ and the relevant constraint from a null measurement is

$$\frac{1}{\sqrt{NH\left(\theta_-\right)}} > \frac{mc^2T}{2\hbar}\left(\xi\left[\frac{2\Lambda^5R_{\rm vac}^2}{M_c^3}\right]^{1/3}-\sqrt{\frac{2\Lambda^5}{M_c\rho_{obj}}}\right)Re^{R/R_{\rm vac}}\left|\frac{e^{-r_1/R_{\rm vac}}}{r_1}-\frac{e^{-r_0/R_{\rm vac}}}{r_0}\right|. \tag{C6}$$

This corresponds to the positively sloped section of Figure 2.

The vertical section occurs when both the massive source and the vacuum in the chamber are screened, which leads to a $\Lambda$-independent field profile and

$$\frac{1}{\sqrt{NH\left(\theta_-\right)}} > \frac{mc^2T}{2\hbar}\left(\frac{\rho_{obj}R^3}{3M_c^2}\right)e^{R/R_{\rm vac}}\left|\frac{e^{-r_1/R_{\rm vac}}}{r_1}-\frac{e^{-r_0/R_{\rm vac}}}{r_0}\right|. \tag{C7}$$

The horizontal boundaries in Figure 3 for early values of $n$ result from the source and the vacuum both being screened. For larger values of $n$, the background field profile given in Eq. (C5) is used.

### 2. Symmetron constraints, Figure 4 in the main text

The value of $\mu_s$ to which these constraints apply is limited by the geometry of the proposed experiment, as the Compton wavelength in low density regions is approximately $1/\mu_s$. For the field to evolve to its vacuum minimum within the chamber, the Compton wavelength

must be smaller than the vacuum chamber radius. However, if the Compton wavelength is too small then the field is Yukawa supressed. The value of $\mu_s$ that this proposed experiment can constrain is restricted by these two conditions to

$$10^{-5.5}\ \text{eV} \lesssim \mu_s \lesssim 10^{-4}\ \text{eV} \tag{C8}$$

in natural units.

An object is screened from the symmetron force when its density is above the critical density $\rho_* = \mu_s^2 M_s^2$. The region in $M_s$ that our proposed experiment would constrain is the region where this critical density is between the densities of the source object and the surrouding vacuum. These two density restrictions cause the sharp sides of the excluded regions in both our predicted excluded regions and the atom interferometry exclusion regions in Figure 4.

The curve in the high $M_s$ section of the predicted excluded regions is the area where the critical density and the source object density become comparable. The peak in the low $M_s$ section of the $\mu_s = 10^{-4}$ eV excluded region is caused by a resonance where the Compton wavelength of the symmetron field matches the distance from the object to the BEC.

The wavefunctions of atoms in a BEC are (in the ideal case) spread over the width of the BEC and all overlap. As a first approximation, we consider the BEC to be a region of uniform density as opposed to a collection of discrete objects. The density of the BEC is between that of the vacuum and the source object. When the BEC density is below the critical density, it does not substantially modify the symmetron field profile. When the BEC density is above the critical density, there should in principle be a dip in the symmetron field profile. However, the Compton wavelength of the symmetron is far greater than the width of the BEC in this entire section of the parameter space, so the BEC again does not substantially effect the symmetron field profile. Hence, whether or not the BEC is screened does not play a role in determining the region of parameter space excluded by our proposed experiment.

The full bound is given by

$$\begin{aligned}\frac{1}{\sqrt{NH\left(\theta_-\right)}} > \frac{mc^2T}{2\hbar}\frac{\mu_s^2}{\lambda M_s^2}\left(1-\frac{\rho_\infty}{\mu_s^2 M_s^2}\right)\times \\ \left(2\Gamma\left[\frac{e^{-m_{out}r_0}}{r_0}-\frac{e^{-m_{out}r_1}}{r_1}\right]+\Gamma^2\left[\frac{e^{-2m_{out}r_1}}{r_1^2}-\frac{e^{-2m_{out}r_0}}{r_0^2}\right]\right)\end{aligned} \tag{C9}$$

where

$$\Gamma = Re^{m_{out}R}\frac{m_{in}R - \tanh\left(m_{in}R\right)}{m_{in}R + m_{out}R\tanh\left(m_{in}R\right)} \tag{C10}$$

and

$$m_i^2 = 2\left(\mu_s^2 - \frac{\rho_i}{M_s^2}\right). \tag{C11}$$

---


[1] C. Brans and R. H. Dicke, Phys. Rev. **124**, 925 (1961).

[2] Y. Fujii and K. Maeda, *The scalar-tensor theory of gravitation*, Cambridge Monographs on Mathematical Physics (Cambridge University Press, 2007).

[3] I. K. Wehus and F. Ravndal, Int. J. Mod. Phys. **A19**, 4671 (2004), arXiv:hep-ph/0210292 [hep-ph].

[4] S. Perlmutter *et al.* (Supernova Cosmology Project), Astrophys. J. **517**, 565 (1999), arXiv:astro-ph/9812133 [astro-ph].

[5] A. G. Riess *et al.* (Supernova Search Team), Astron. J. **116**, 1009 (1998), arXiv:astro-ph/9805201 [astro-ph].

[6] T. Clifton, P. G. Ferreira, A. Padilla, and C. Skordis, Phys. Rept. **513**, 1 (2012), arXiv:1106.2476 [astro-ph.CO].

[7] A. Joyce, B. Jain, J. Khoury, and M. Trodden, Phys. Rept. **568**, 1 (2015), arXiv:1407.0059 [astro-ph.CO].

[8] J. O. Dickey, P. L. Bender, J. E. Faller, X. X. Newhall, R. L. Ricklefs, J. G. Ries, P. J. Shelus, C. Veillet, A. L. Whipple, J. R. Wiant, J. G. Williams, and C. F. Yoder, Science **265**, 482 (1994).

[9] E. G. Adelberger, B. R. Heckel, and A. E. Nelson, Annu. Rev. Nucl. Part. S. **53**, 77 (2003).

[10] D. J. Kapner, T. S. Cook, E. G. Adelberger, J. H. Gundlach, B. R. Heckel, C. D. Hoyle, and H. E. Swanson, Phys. Rev. Lett. **98**, 021101 (2007).

[11] M. Ishak, Living Rev. Rel. **22**, 1 (2019), arXiv:1806.10122 [astro-ph.CO].

[12] C. Burrage and J. Sakstein, Living Rev. Rel. **21**, 1 (2018), arXiv:1709.09071 [astro-ph.CO].

[13] A. D. Ludlow, M. M. Boyd, J. Ye, E. Peik, and P. O. Schmidt, Rev. Mod. Phys. **87**, 637 (2015).

[14] D. Schlippert, H. Albers, L. L. Richardson, D. Nath, H. Heine, C. Meiners, E. Wodey, A. Bil-

lon, J. Hartwig, C. Schubert, N. Gaaloul, W. Ertmer, and E. M. Rasel, Proceedings of the 50th Rencontres de Moriond "Gravitation: 100 years after GR", La Thuile (Italy) (2015).

[15] C. Overstreet, P. Asenbaum, T. Kovachy, R. Notermans, J. M. Hogan, and M. A. Kasevich, Phys. Rev. Lett. **120**, 183604 (2018).

[16] D. Becker, M. D. Lachmann, S. T. Seidel, H. Ahlers, A. N. Dinkelaker, J. Grosse, O. Hellmig, H. Müntinga, V. Schkolnik, T. Wendrich, A. Wenzlawski, B. Weps, R. Corgier, T. Franz, N. Gaaloul, W. Herr, D. Lüdtke, M. Popp, S. Amri, H. Duncker, M. Erbe, A. Kohfeldt, A. Kubelka-Lange, C. Braxmaier, E. Charron, W. Ertmer, M. Krutzik, C. Lämmerzahl, A. Peters, W. P. Schleich, K. Sengstock, R. Walser, A. Wicht, P. Windpassinger, and E. M. Rasel, Nature **562**, 391 (2018).

[17] C. Burrage, E. J. Copeland, and E. A. Hinds, JCAP **1503**, 042 (2015), arXiv:1408.1409 [astro-ph.CO].

[18] M. Jaffe, P. Haslinger, V. Xu, P. Hamilton, A. Upadhye, B. Elder, J. Khoury, and H. Müller, Nature Physics **13**, 938 (2017).

[19] D. Hartley, C. Käding, R. Howl, and I. Fuentes, Phys. Rev. D **99**, 105002 (2019).

[20] C. Burrage and J. Sakstein, Journal of Cosmology and Astroparticle Physics **2016**, 045 (2016).

[21] J. Khoury and A. Weltman, Phys. Rev. **D69**, 044026 (2004), arXiv:astro-ph/0309411 [astro-ph].

[22] J. Khoury and A. Weltman, Phys. Rev. Lett. **93**, 171104 (2004), arXiv:astro-ph/0309300 [astro-ph].

[23] H. Dehnen, H. Frommert, and F. Ghaboussi, International Journal of Theoretical Physics **31**, 109 (1992).

[24] E. Gessner, Astrophysics and Space Science **196**, 29 (1992).

[25] T. Damour and A. M. Polyakov, Nucl. Phys. **B423**, 532 (1994), arXiv:hep-th/9401069 [hep-th].

[26] M. Pietroni, Phys. Rev. D **72**, 043535 (2005).

[27] K. A. Olive and M. Pospelov, Phys. Rev. D **77**, 043524 (2008).

[28] P. Brax, C. van de Bruck, A.-C. Davis, and D. Shaw, Phys. Rev. D **82**, 063519 (2010).

[29] K. Hinterbichler and J. Khoury, Phys. Rev. Lett. **104**, 231301 (2010), arXiv:1001.4525 [hep-th].

[30] K. Hinterbichler, J. Khoury, A. Levy, and A. Matas, Phys. Rev. **D84**, 103521 (2011),

arXiv:1107.2112 [astro-ph.CO].

[31] C. Burrage, A. Kuribayashi-Coleman, J. Stevenson, and B. Thrussell, JCAP **1612**, 041 (2016), arXiv:1609.09275 [astro-ph.CO].

[32] Y. Shin, M. Saba, T. A. Pasquini, W. Ketterle, D. E. Pritchard, and A. E. Leanhardt, Phys. Rev. Lett. **92**, 050405 (2004).

[33] J. E. Debs, P. A. Altin, T. H. Barter, D. Döring, G. R. Dennis, G. McDonald, R. P. Anderson, J. D. Close, and N. P. Robins, Phys. Rev. A **84**, 033610 (2011).

[34] T. Berrada, S. van Frank, R. Bücker, T. Schumm, J.-F. Schaff, and J. Schmiedmayer, Nature Communications **4**, 2077 (2013).

[35] H. Müntinga, H. Ahlers, M. Krutzik, A. Wenzlawski, S. Arnold, D. Becker, K. Bongs, H. Dittus, H. Duncker, N. Gaaloul, C. Gherasim, E. Giese, C. Grzeschik, T. W. Hänsch, O. Hellmig, W. Herr, S. Herrmann, E. Kajari, S. Kleinert, C. Lämmerzahl, W. Lewoczko-Adamczyk, J. Malcolm, N. Meyer, R. Nolte, A. Peters, M. Popp, J. Reichel, A. Roura, J. Rudolph, M. Schiemangk, M. Schneider, S. T. Seidel, K. Sengstock, V. Tamma, T. Valenzuela, A. Vogel, R. Walser, T. Wendrich, P. Windpassinger, W. Zeller, T. van Zoest, W. Ertmer, W. P. Schleich, and E. M. Rasel, Phys. Rev. Lett. **110**, 093602 (2013).

[36] G. D. McDonald, C. C. N. Kuhn, K. S. Hardman, S. Bennetts, P. J. Everitt, P. A. Altin, J. E. Debs, J. D. Close, and N. P. Robins, Phys. Rev. Lett. **113**, 013002 (2014).

[37] A. D. Cronin, J. Schmiedmayer, and D. E. Pritchard, Rev. Mod. Phys. **81**, 1051 (2009).

[38] M. Albiez, R. Gati, J. Fölling, S. Hunsmann, M. Cristiani, and M. K. Oberthaler, Phys. Rev. Lett. **95**, 010402 (2005).

[39] D. S. Naik, G. Kuyumjyan, D. Pandey, P. Bouyer, and A. Bertoldi, Quantum Science and Technology **3**, 045009 (2018).

[40] T. Berrada, S. van Frank, R. Bücker, T. Schumm, J.-F. Schaff, J. Schmiedmayer, B. Julía-Díaz, and A. Polls, Phys. Rev. A **93**, 063620 (2016).

[41] S. L. Braunstein and C. M. Caves, Phys. Rev. Lett. **72**, 3439 (1994).

[42] M. G. A. Paris, International Journal of Quantum Information **07**, 125 (2009).

[43] D. Šafránek and I. Fuentes, Phys. Rev. A **94**, 062313 (2016).

[44] A. Monras, Phys. Rev. A **73**, 033821 (2006).

[45] O. Pinel, P. Jian, N. Treps, C. Fabre, and D. Braun, Physical Review A **88**, 040102(R) (2013).

[46] D. Šafránek, A. R. Lee, and I. Fuentes, New Journal of Physics **17**, 073016 (2015).

[47] P. Kok and B. W. Lovett, *Introduction to optical quantum information processing* (Cambridge University Press, 2010).

[48] K. M. R. van der Stam, E. D. van Ooijen, R. Meppelink, J. M. Vogels, and P. van der Straten, Review of Scientific Instruments **78**, 013102 (2007), https://doi.org/10.1063/1.2424439.

[49] D. G. Fried, T. C. Killian, L. Willmann, D. Landhuis, S. C. Moss, D. Kleppner, and T. J. Greytak, Phys. Rev. Lett. **81**, 3811 (1998).

[50] T. Greytak, D. Kleppner, D. Fried, T. Killian, L. Willmann, D. Landhuis, and S. Moss, Physica B: Condensed Matter **280**, 20 (2000).

[51] G.-B. Jo, Y. Shin, S. Will, T. A. Pasquini, M. Saba, W. Ketterle, D. E. Pritchard, M. Vengalattore, and M. Prentiss, Phys. Rev. Lett. **98**, 030407 (2007).

[52] S. Zhou, D. Groswasser, M. Keil, Y. Japha, and R. Folman, Phys. Rev. A **93**, 063615 (2016).

[53] P. Hamilton, M. Jaffe, P. Haslinger, Q. Simmons, H. Müller, and J. Khoury, Science **349**, 849 (2015).

[54] G. R. Dvali, G. Gabadadze, and M. Porrati, Phys. Lett. **B485**, 208 (2000), arXiv:hep-th/0005016 [hep-th].

[55] T. Damour and A. M. Polyakov, Nucl. Phys. **B423**, 532 (1994), arXiv:hep-th/9401069 [hep-th].

[56] P. Brax, C. van de Bruck, A.-C. Davis, B. Li, and D. J. Shaw, Phys. Rev. **D83**, 104026 (2011), arXiv:1102.3692 [astro-ph.CO].

[57] S. Fagnocchi, S. Finazzi, S. Liberati, M. Kormos, and A. Trombettoni, New Journal of Physics **12**, 095012 (2010).

[58] D. Hartley, T. Bravo, D. Rätzel, R. Howl, and I. Fuentes, Phys. Rev. D **98**, 025011 (2018).

[59] L. Pitaevskii and S. Stringari, *Bose-Einstein Condensation* (Oxford University Press, 2003).

[60] C. J. Pethick and H. Smith, *Bose-Einstein Condensation in Diulte Gases* (Cambridge University Press, 2002).

[61] B. Elder, J. Khoury, P. Haslinger, M. Jaffe, H. Mller, and P. Hamilton, Phys. Rev. **D94**, 044051 (2016), arXiv:1603.06587 [astro-ph.CO].